High-Pressure Ablation Measurements in the AEDC Track G

J. J. Matty*
Arnold Engineering Development Center, Arnold Air Force Station, Tennessee

The Track G version of the ABRES Shape Change Code (ASCC-G) is used to predict the surface ablation and temperature distribution as well as the bow shock shape and location for several shots in the AEDC Track G facility. The predictions are compared with data, and an explanation offered for the apparent underprediction of recession as well as the apparent overprediction of the model surface temperature. This explanation suggests that the helium environments used at the Track G image-converter stations may bias both recession and temperature data, resulting in significant deviations from the code predictions.

Nomenclature

B = bias limit
c_2 = constant in Eq. (7), cm-K
c_p = specific heat at constant pressure, Btu/lbm-°R
DEL = ASCC internal grid point spacing, in.
D_p = distance from receding surface to a point at which the temperature drops to 10 percent of surface temperature, in.
H_0 = stagnation enthalpy, Btu/lbm
i = integer
K = thermal conductivity, Btu/ft-s-°R
k = Physical peak-to-valley roughness element height, mils
L_a = model axial length, in.
L_r = model radial thickness, in.
N = number of measurements
P_0' = model stagnation pressure, atm
P_∞ = static pressure, atm
$Re_{\theta,TR}$ = transition Reynolds number, $\theta\rho V/\mu$
R_n = model nose radius, in. (unablated)
S = precision index
s = model stagnation point recession, in.
$\dot{s}$ = model stagnation point recession rate, in./s
T = temperature, K
$\bar{T}$ = average temperature value, K
T_{br} = brightness temperature, K
T_e = boundary-layer edge temperature, K
T_i = individual temperature measurement, K
T_w = wall temperature, K
t = time, s
U = uncertainty of temperature measurement, K
V = velocity, ft/s
V_∞ = free-stream velocity, ft/s
α = thermal diffusivity, ft²/s
β = model internal grid point angle, deg
$\epsilon(\lambda,T)$ = emissivity of the material at λ and T
θ = momentum thickness, mils
λ = wavelength, Å
μ = viscosity, lbm/s-ft
ρ = density, lbm/ft³

Introduction

An area of continued interest in the aerodynamic arena is the thermophysics associated with high-speed re-entry vehicles. The large heat loads produced in re-entry can be dealt with either by active cooling, such as water or gas expulsion, or passively through ablation of the thermal protection material. The resultant shape change of the passively protected entry body as well as the subsequent mass loss into the free stream will affect the flowfield and the aerodynamic forces on the body. Efforts to predict the ablative shape change include model testing in high-velocity ranges and application of computational aerodynamic models. The AEDC Hypervelocity Range/Track G facility has been used for this type of testing in conjunction with the Advanced Ballistic Re-entry System (ABRES) Shape Change Code (ASCC). This testing has mostly been conducted with the range at atmospheric or subatmospheric conditions; however, in the past two years, a requirement to test thermal protection materials at even higher pressures has become necessary. To meet these conditions, a relatively new technique has been used which involves pressurizing the Track G facility to obtain very high model stagnation pressure during the test. The ABRES Shape Change Code has been applied in the present work as a tool to predict the shape change, bow shock shape and location, as well as the surface temperature contours of a model in the Track G facility at these high pressures. This paper covers the results from the test and compares them with the code's predictions. Then an explanation is suggested to account for the observed differences.

Test Unit

Track G is 1600 ft long (see Fig. 1) and consists of the following major components: 1) the model launcher, which is a two-stage, 2.5-in.-bore powder and hydrogen gas gun 150 ft in length, 2) the 923-ft track portion, which provides model guidance through the test environment and enables recovery, 3) the 500-ft model recovery tube, which aerodynamically stops the model through the use of pressurized helium and nitrogen gas, 4) the 1000-ft range tank, which surrounds the track section and can be pressurized or evacuated as necessary with various gases to produce the proper environment for the test, and 5) the instrumentation system, which takes the laser and image-converter photographs. The range tank is divided by bulkheads at 45 and 345 ft from the end of the launcher. The openings in the bulkheads through which the track passes are equipped with quick-opening valves which allow three distinct pressure levels along the range. Reference 1 contains a more complete description of the track system and its operation. By removing the track, the facility is also used as a free-flight range.

Instrumentation

A variety of instrument systems are used in Track G including high-speed photopyrometry and photography. Approximately six photopyrometer stations and 12 laser

Presented as Paper 84-1804 at the AIAA 19th Thermophysics Conference, Snowmass, CO, June 25-28, 1984; received Aug. 6, 1984; revision received May 30, 1985. This paper is declared a work of the U. S. Government and therefore is in the public domain.

*Re-entry Systems Test Engineer, Re-entry Branch, Analysis Division, Aerospace Flight Dynamics Directorate, AEDC. Member AIAA.

photography stations were located in the Track G facility to obtain data for the subject test.

Photopyrometry

A typical pyrometer station along Track G is shown in Fig. 2. Two basic types of image-intensifier cameras are available. The Gen-I camera, developed in 1975, covers the temperature range from approximately 1500 to 4500 K, and the Gen-II camera, developed in 1976, covers the temperature range from approximately 1200 to 2000 K. The image-intensifier camera (IC) takes a high-speed, self-luminous photograph of the model nosetip. The same film is exposed to a reference temperature source and processed on a high-speed, digital-scanning microdensitometer. A data reduction program then uses the reference temperature information and a density/temperature calibration curve to produce isothermal contour maps (see Fig. 3). Horizontal and vertical temperature scans of the contour maps are also produced. A thorough description of this system can be found in Refs. 2 and 3.

Laser Photography

Laser photographs are taken with an open-shutter, pulsed-flash system shown schematically in Fig. 4. The exposure time of 20 ns provides high-quality, stop-motion photographs of shock shape and location as well as surface recession history.

Model Description

The model for this test series, representing the entry vehicle nosetip only, was a carbonaceous sphere cone adapted for use with the cruciform track configuration. A model is shown in Fig. 5.

Theoretical Model

The theoretical model used to predict the shape change, bow shock shape and location, and surface temperature data from the present test is the Track G version of the ABRES Shape Change Code (ASCC-G). The main inputs to the code are the material properties, the model configuration, the free-stream conditions, and the model velocity-time history. The major computational elements of the code that are used in the present analysis are the inviscid solution, viscous solution, surface mass/energy balance, and in-depth transient heat conduction. The resultant shape change, in-depth temperatures, and flowfield characteristics are calculated as the program moves forward in time (see Fig. 6). The inviscid calculations are made by dividing the nosetip into three regions: stagnation point to sonic point, sonic point to aft shoulder, and aft shoulder to the end of the nosetip. The surface pressure ratio is then calculated over each region using semiempirical relationships.

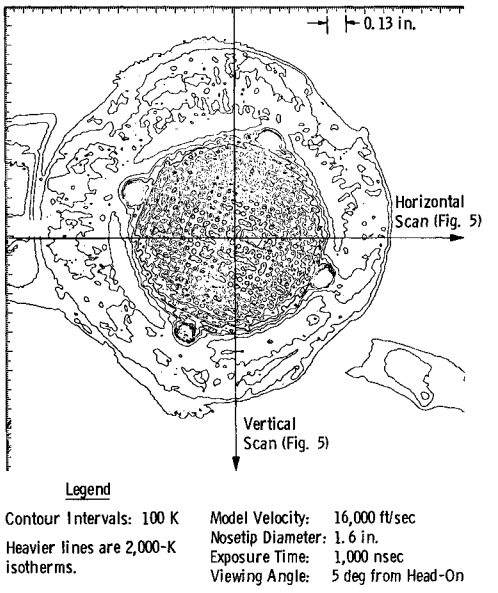

Fig. 3 Isothermal contour map of nosetip-Gen-I photopyrometer.

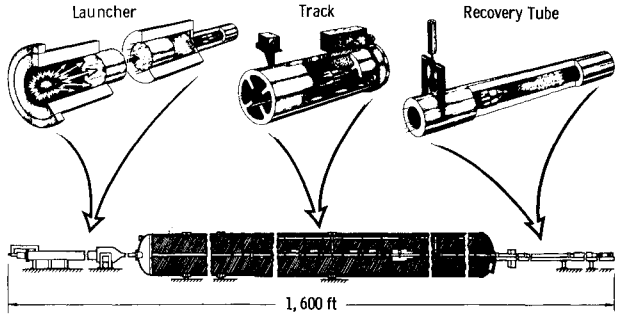

Fig. 1 AEDC hypervelocity range/track (G).

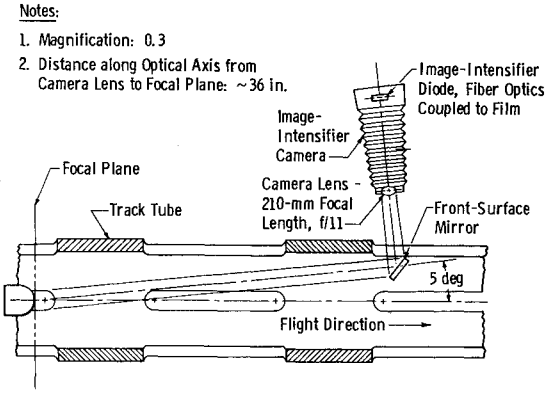

Fig. 2 Track photopyrometer arrangement.

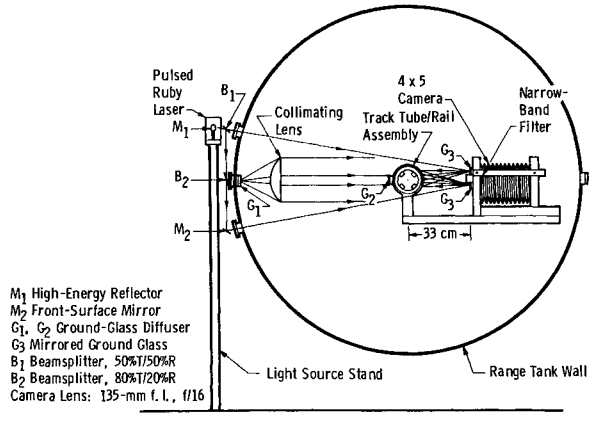

Fig. 4 Track G front-light/back-light laser photography system.

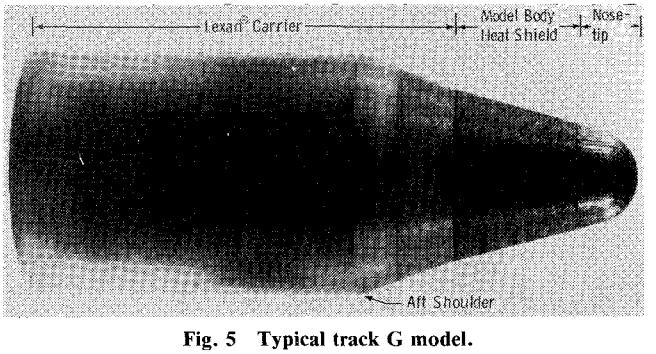

Fig. 5 Typical track G model.

The viscous portion of the code uses a simultaneous solution of the momentum/energy integral equations modified for the re-entry vehicle conditions through the use of influence coefficients. These coefficients account for flow acceleration, surface roughness, and transition proximity. The surface energy balance is computed between the following: 1) sensible convective heat flux, 2) chemical energy flux, 3) radiative heat flux, 4) energy attributable to movement of the control volume into the model and, 5) conduction heat flux. A more complete description of the basic 1976 version of the code is found in Ref. 4.

Test Procedures

The test technique used in this experiment involves launching a model along the Track G into a clear-air, high-pressure environment. The test models were launched at approximately 17,000 ft/s into air at a pressure of 0.4 atm for the first 300 ft and 1.7 atm for the remaining 575 ft of the range tank. This combination of initial velocity and range pressures produced the velocity profile and stagnation properties shown in Fig. 7.

Measurement Uncertainty

The two major measurement systems used in the Track G facility are the laser photographs and the image-converter cameras or photopyrometers. The recession uncertainty associated with the individual laser photograph measurement is estimated at ±3 mil. The uncertainty in the model brightness temperature distribution, which is described below, is a sum of the errors associated with both the pyrometer measurement system and the test article.

Photopyrometer System Uncertainty

Although factors such as film-to-film inconsistency, film processing variations, and microdensitometer imprecision may contribute to uncertainty in the pyrometer measurement system, the major contributors are the calibration source and the calibration curve-fit uncertainties. The calibration source uncertainty is estimated in magnitude at ±15 K, and the error associated with using a straight line, rather than a polynomial, to curve fit the calibration data is estimated at ±20 K. The National Bureau of Standards method for calculating the uncertainty assumes

$$U = \pm (B + t_{95}S) \tag{1}$$

where B is the bias limit, S is the precision index, and t_{95} is the 95th percentile point for the two-tailed Student's "t" distribution.[5] The bias term, B, is calculated as simply the root sum square of the two errors listed above, i.e.,

$$B = \pm\sqrt{(15\,K)^2 + (20\,K)^2} \tag{2}$$

or

$$B = \pm 25K \tag{3}$$

The precision index, S, which is an estimate of the standard deviation, is given by

$$S = \sqrt{\left[\sum_{i=1}^{N} (T_i - \bar{T})^2\right] \Big/ (N-1)} \tag{4}$$

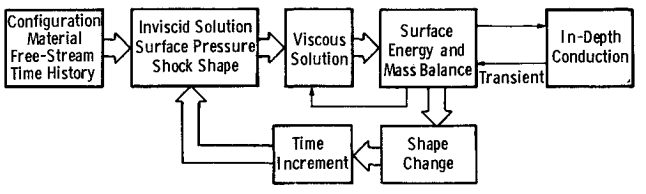

Fig. 6 ASCC computational elements.

where N is the number of measurements made, T_i are the individual measurements, and $\bar{T}$ is the average value. The statistical value of t_{95} is a function of N. These values are then combined in Eq. (1) to yield the values of uncertainty, U, graphed in Fig. 8 as a function of temperature, the type of camera used, and the exposure time.[3]

Test Article Associated Uncertainty

Uncertainty sources associated with the test article include: 1) motion blur, 2) chemiluminescence, 3) shock-cap air radiation, 4) heat-shield luminosity, 5) wake radiation, and 6) nosetip hot spots.[3] Steps have been taken to minimize these errors, including the use of helium at the photopyrometer stations described below.

In cases where the shock-cap brightness temperature exceeds the model surface temperatures, as in the subject test, a short helium gas filled area is provided to reduce the shock-cap radiation level below the threshold of the photopyrometers. The gas is injected below the track just prior to the pyrometer station and provides up to 95% pure helium over a flight distance of approximately 46 in. This inert helium environment quenches, or temporarily suspends, the oxidation process which would normally result in chemilu-

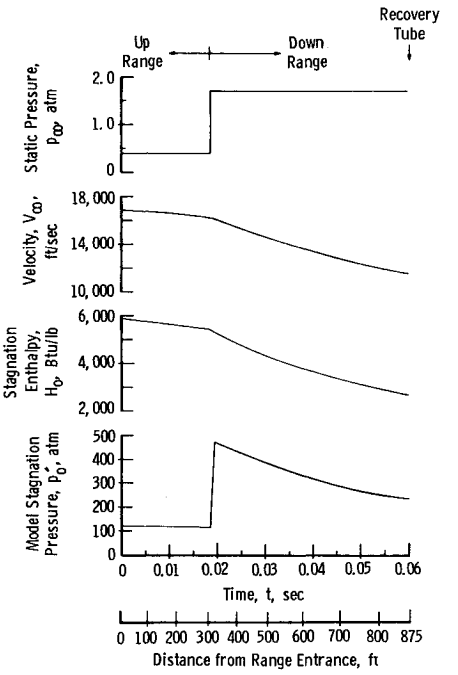

Fig. 7 Test conditions.

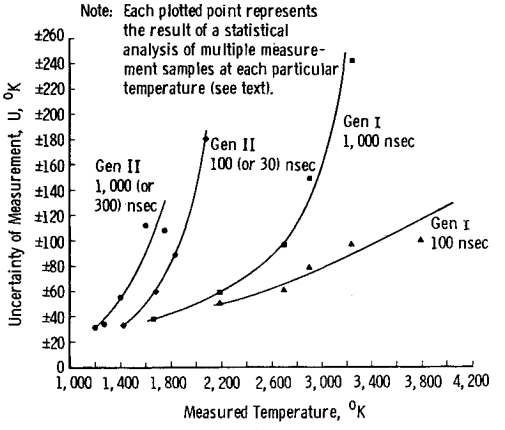

Fig. 8 Photopyrometer temperature measurement uncertainty.

minescence, i.e., luminescence resulting from the chemical processes involved.[6]

Theoretical Model Application

The first step in applying the theoretical model is laying out the computational mesh. The fixed polar coordinates cover the flow-field computational area, and the internal grid points cover the test article (see Fig. 9). The depth to be covered by the internal grid point layout was calculated through the use of a steady-state analysis of a semi-infinite solid with constant surface heat flux and recession rate as follows:

$$D_p = \frac{2.3\alpha}{\dot{s}} \tag{5}$$

and

$$\alpha = \frac{k}{\rho c_p} \tag{6}$$

where α is the material thermal diffusivity, k is the thermal conductivity, ρ the density, c_p the specific heat at constant pressure, and D_p the distance from the receding surface to the point within the model where the temperature drops to 10% of the surface temperature. Acceptable layouts were achieved for both the fixed polar and the internal grid point systems.

Several options are available within the code to handle boundary-layer transition. The decision to use the code's abrupt turbulent-boundary-layer input option, which assumes a turbulent boundary layer throughout the run, was based on correlations of previous ballistic range experiments by D. Reda.[7] The surface thermochemistry tables input into the ASCC-G were generated by the Aerotherm Chemical Equilibrium (ACE) program.[8]

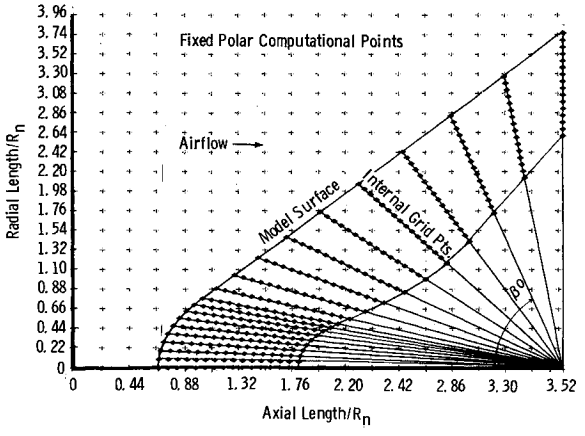

Fig. 9 ASCC computational grid layout.

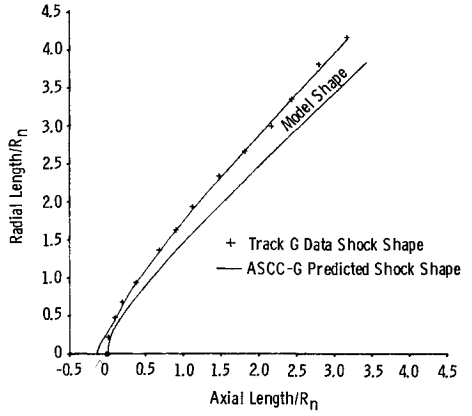

Fig. 10 Bow shock shape and location vs theory.

Experimental/Theoretical Results

The measurable parameters from the test were compared with the ASCC-G predictions and include bow shock shape and location, stagnation point recession, and model brightness temperature profiles. Over 30 high-pressure (0.4-1.7 atm), ablation shots have been conducted in Track G. Of these, the largest group, with almost identical model configurations and test conditions, contained six shots. Although the comparisons were completed on each of these shots, only a representative shot is presented here.

Bow Shock Shape and Location

Bow shock shape and location were read directly from the laser photographs. To avoid the problem of having the code predict a shock on a predicted model shape, the actual ablated model profile at a given laser station was digitized, input into the ASCC-G, and "frozen" by selecting a no-shape-change option. The code predicted the shock shape and location at the appropriate laser station (see Fig. 10). The prediction agrees well with the data with the exception of the area near the nosetip which may be due to the coarse computational grid layout relative to rapid changes in the flowfield in that area. Because of the nature of the code, when an exact model profile is input, as in this case, the code lays out the computational grids automatically with no provisions for variation as were made in the following stagnation point recession calculations.

Stagnation Point Recession

The stagnation point recession data from the laser photographs are compared to the ASCC-G predictions in Fig. 11. Even though the curves show similar trends, the prediction is consistently below the data. Hence, checks were made on the internal grid point spacing. Calculations using 2, 2.5, and 3 times the calculated minimum required spacing yielded little change. The solution's insensitivity to grid changes suggested a proper grid layout. More will be said about the difference noted here between theory and data in the discussion of the model surface temperature measurements.

Model Brightness Temperatures

The high-speed image-converter photographs produce model brightness temperature T_{br} profiles. This brightness temperature is related to the actual model surface temperature T by the following relation which is derived from Planck's formula:

$$\ell n \epsilon(\lambda, T) = \frac{c_2}{\lambda}\left(\frac{1}{T} - \frac{1}{T_{br}}\right) \tag{7}$$

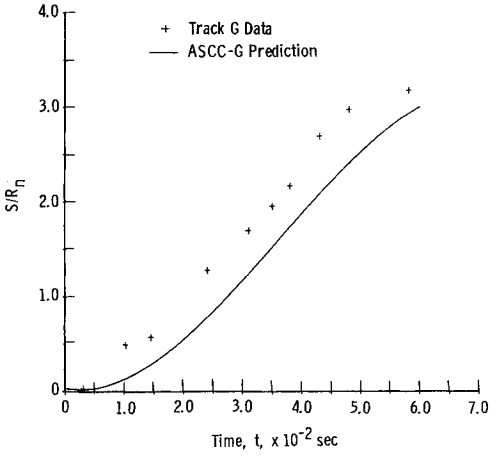

Fig. 11 Stagnation point recession vs theory.

where $c_2 = 1.4350$ cm-K (international temperature scale of 1948).[9] For the pyrometers used in the Track G facility, a typical spectral response curve ranges between 5300 and 9000 Å. The emissivity of the test material is assumed constant with respect to the wavelength and temperature. With an emissivity value of 1.0, the brightness temperature is equal to the surface temperature by Eq. (7). Figure 12 shows the possible differences between the brightness temperature and the surface temperature ΔT as a function of emissivity. Note that there is very little temperature deviation between the extremes of the pyrometer response wavelengths such that, if the actual material emissivity varies from 1.0, the effect on the relationship between the brightness and true temperature is relatively small.

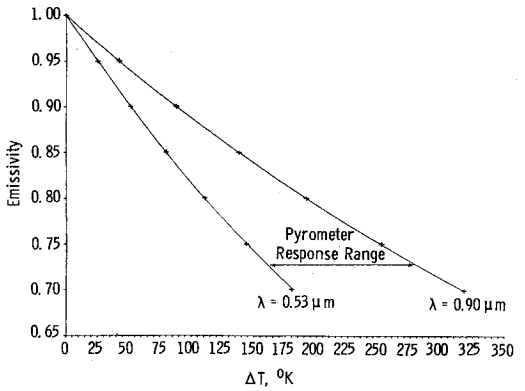

Fig. 12 Emissivity effect on brightness temperature to true temperature conversion.

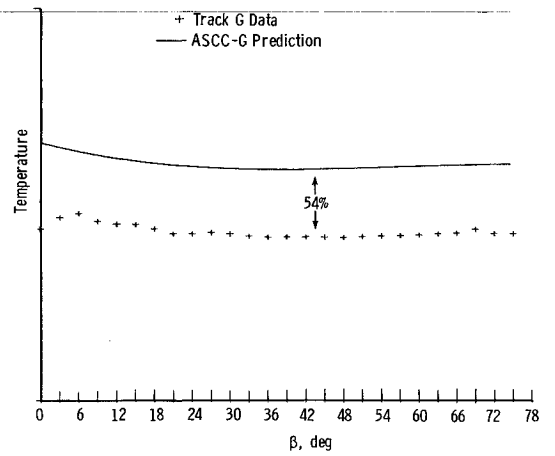

Fig. 13 Circumferentially averaged surface temperature vs theory (IC 4).

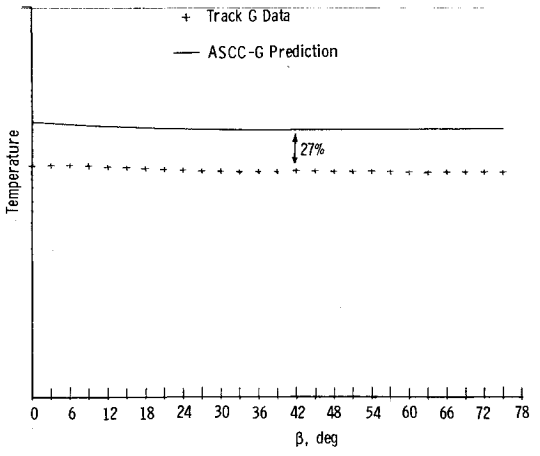

Fig. 14 Circumferentially averaged surface temperature vs theory (IC 20).

The profile of model brightness temperature as measured by the image-converter cameras is circumferentially averaged and presented in terms of degrees Beta, where 0 deg corresponds to the model stagnation point (see Fig. 9). The results are shown in Figs. 13 and 14 for two data stations spaced 300 ft apart. The emissivity of the nosetip material is assumed to be unity. In both cases, the theoretical prediction is well above the data.

To check proper code usage, the predictions of the stagnation temperatures for several low-pressure shots were made with good results as shown in Fig. 15. The following avenues were explored to account for the apparent discrepancy in the high-pressure predictions: 1) possible errors resulting from stagnation point identification during data reduction, 2) alterations to the data reduction algorithm to account for exact model shape, 3) improper chemical modeling within the code and, 4) possible data biasing by the helium shock-cap quench technique used in conjunction with the temperature measurement system.

The stagnation point is located manually during the data reduction process and provides the reference point for all other temperature measurements. In an attempt to reduce any repeatability errors associated with this process, the surface stagnation point temperature was averaged over areas enclosed by radii from 0.050 to 0.10 in. with very little effect.

The isothermal contour maps produced by the surface-temperature data reduction program had been designed originally for cut-sphere nosetips. The program was modified to account for the sphere-cone configuration of the present model, again with very little effect.

Another possible explanation for the data-theory mismatch relates to the material thermochemical properties input into the code. These may not apply at the temperatures and pressures encountered during this test. This possibility was explored by K. M. Kratsch, et al.[10] who concluded that stagnation pressures as low as 100 atm can produce an experimental mass flux from a carbon model that is about a factor of two greater than predicted by thermochemical erosion alone. Surprisingly, he noted that this increased mass loss resulted in a rather small decrease in surface temperatures.

Another area investigated was the possible effect of the helium gas used to quench the shock cap. This possibility has also been suggested by C. Park of the NASA Ames Research Center concerning work he has done with range data using argon as the test gas.[11] Figure 16 shows an oblique-view image-converter photograph of a Track G model under high-pressure conditions with no helium gas at this station (note the radiation visible from the shock cap). Figure 17 shows another

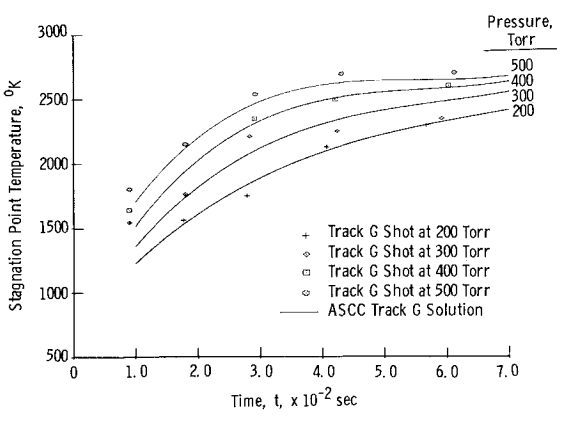

Fig. 15 ASCC-G predictions of low-pressure stagnation temperatures.

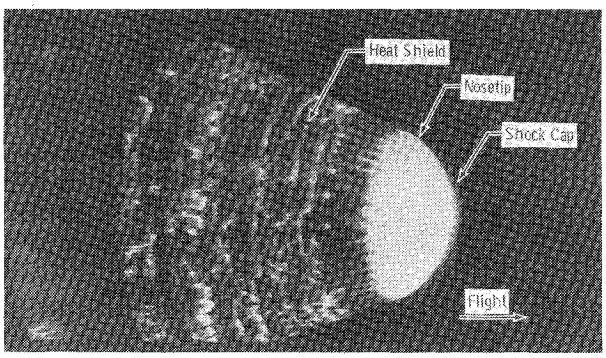

Fig. 16 Image-converter photograph without helium.

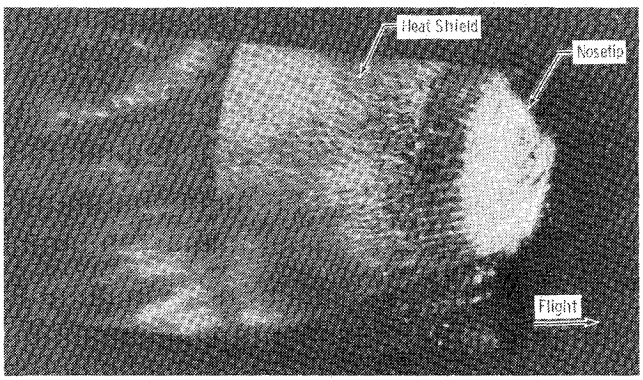

Fig. 17 Image-converter photograph with helium.

Track G model with the nosetip from the same billet of material as it passes the same image-converter station. The range conditions are virtually identical. The only difference is the body heat-shield material (see Fig. 5) and the fact that the helium gas is used on this shot to quench the shock cap. The apparent material loss from the nosetip is similar on all image-converter photographs taken during this flight. Calculations of the dynamic pressure difference experienced by the model surface upon entry into the helium reveal a drop to about one-seventh the level in air. As many of the materials tested were porous by design, it is conceivable that an abrupt decrease in pressure on the surface could cause a material ejection as the gases expand to equalize pressure.

The ASCC-G predicts internal temperatures at each of the points shown within the model (Fig. 9) and predicts a very steep gradient at the surface throughout the model flight. A simple calculation was performed to determine how far into the model surface (at the stagnation point) one would have to go to reach temperatures equivalent to the measured surface temperature data. The resulting distance was on the order of the underprediction shown in Fig. 11. This was the case in every shot studied at almost every IC station. Hence, the step decrease in dynamic pressure on the model (upon entering the helium environment) may result in more model recession than predicted, as shown in Fig. 11, as well as a decrease in measured model surface temperature because the hot surface is ejected and the cooler surface exposed just prior to the image-converter photograph. This possibility as well as other potential error sources noted are being investigated further at AEDC.

Conclusions

A relatively new testing technique involving pressurization of the AEDC Track G facility has been developed. Representative data when compared to the ASCC-G theoretical predictions show good agreement on shock shape and location, but the code underpredicts stagnation point recession and overpredicts model surface temperature by 30 to 50%. Several explanations are being investigated at this time, with the helium shock-cap quench effects being the most probable explanation.

Acknowledgments

The author wishes to express his sincere thanks to the test project engineer, Randall Watt, and his associates at Arnold Center for carrying out the tests and reducing the basic data used in the present work. Also, appreciation is extended to Emmett Edenfield and Brad Brown for their help with the ASCC and data plots.

This work was accomplished by the Arnold Engineering Development Center (AEDC), Air Force Systems command (AFSC). Further reproduction is authorized to satisfy needs of the U. S. Government.

References

[1]Norfleet, G. D., Hendrix, R. E., and Jackson, D., "Development of a Hypervelocity Track Facility at AEDC," AIAA Paper 77-151, 15th Aerospace Sciences Meeting, Los Angeles, CA, Jan. 1977.

[2]"Von Kármán Gas Dynamics Facility, Vol. 3," Arnold Engineering Development Center, Arnold AFS, TN, April 1981, pp. 7.4-7.6.

[3]Dugger, P. H., Enis, C. P., and Hendrix, R. E., "Aeroballistics Range Photopyrometry," AEDC-TR-82-1 (AD-A111260), Feb. 1982.

[4]Thompson, R. A., and Lewis, C. H. "Effects of Weather Encounters on Aero-Lift Reentry Vehicles," AIAA Paper 82-0858, June 1982.

[5]Eisenhart, C., "Expression of Uncertainties of Final Results, Precision Measurement and Calibration," *NBS Handbook 91,* Vol. I, Boulder, CO, Feb. 1969, pp. 69-72.

[6]Seigel, R. and Howel, J. R., *Thermal Radiation Heat Transfer,* McGraw-Hill, New York, 1972, p. 726.

[7]Reda, D. C., "Correlation of Nosetip Boundary-Layer Transition Data Measured in Ballistic-Range Experiments," Sandia Laboratories, SAND79-0649, Albuquerque, NM, Nov. 1979.

[8]Powers, C. A. and Kendall, R. M., "User's Manual: Aerotherm Chemical Equilibrium (ACE) Computer Program," Aerotherm Corporation, Sunnyvale, CA, May 1969.

[9]Reynolds, M. M., Corruccini, R. J., Fulk, M. M., and Burley, R. M., "Radiometry," in *American Institute of Physics Handbook,* edited by Dwight E. Gray, McGraw-Hill, New York, 1963, pp. 6-153.

[10]Kratsch, K. M., Martinez, M. R., Clayton, F. I., Greene, R. B., and Wuerer, J. E., "Graphite Ablation in High-Pressure Environments," AIAA Paper 68-1153, Dec. 1968.

[11]Park, C., "Stagnation-Point Ablation of Carbonaceous Flat Disks, Part 2. Experiment," *AIAA Journal,* Vol. 21, Dec. 1983, pp. 1748-1754.